Dalton Transactions

# Tuning the Excited-State Deactivation Pathways of Dinuclear Ruthenium(II) 2,2'-Bipyridine Complexes Through Bridging Ligand Design



| | |
|---|---|
| Journal: | *Dalton Transactions* |
| Manuscript ID | DT-ART-04-2020-001216.R2 |
| Article Type: | Paper |
| Date Submitted by the Author: | 20-May-2020 |
| Complete List of Authors: | Cerfontaine, Simon; Université catholique de Louvain, Institute of Condensed Matter and Nanosciences<br>Troian-Gautier, Ludovic; Université Libre de Bruxelles (U.L.B.), Laboratoire de Chimie Organique;<br>Wehlin, Sara; University of North Carolina at Chapel Hill, Chemistry<br>Loiseau, Frederique; Universite Grenoble Alpes, DCM<br>Cauët, Emilie; Université Libre de Bruxelles, Service de Chimie Quantique et Photophysique<br>Elias, Benjamin; Université catholique de Louvain, Institute of Condensed Matter and Nanosciences |
| | |

# Tuning the Excited-State Deactivation Pathways of Dinuclear Ruthenium(II) 2,2'-Bipyridine Complexes Through Bridging Ligand Design

Received 00th January 20xx,
Accepted 00th January 20xx

DOI: 10.1039/x0xx00000x

Simon Cerfontaine,[a] Ludovic Troian-Gautier,[b,c] Sara A. M. Wehlin,[c] Frédérique Loiseau,[d] Emilie Cauët,[e] Benjamin Elias[a]*

A detailed photophysical investigation of two dinuclear ruthenium(II) complexes is reported. The two metallic centers were coordinated to a bis-2,2'-bipyridine bridging ligand, connected either through the *para* (**L$_p$**, **D$_p$**) or the *meta* position (**L$_m$**, **D$_m$**). The results obtained herein were compared to the prototypical $[Ru(bpy)_3]^{2+}$ parent compound. The formation of dinuclear complexes was accompanied by the expected increase in molar absorption coefficients, *i.e.* 12000 $M^{-1}cm^{-1}$, 17000 $M^{-1}cm^{-1}$, and 22000 $M^{-1}cm^{-1}$ at the lowest energy $MLCT_{max}$ transition for $[Ru(bpy)_3]^{2+}$, **D$_m$** and **D$_p$** respectively. The **L$_p$** bridging ligand resulted in a ruthenium (II) dinuclear complex that absorbed more visible light, had a longer-lived and more delocalized excited-state compared to a complex with the **L$_m$** bridging ligand. Variable temperature measurements provided valuable information about activation energies to the uppermost $^3$MLCT state and the metal-centered ($^3$MC) state, often accompanied by irreversible ligand-loss chemistry. At 298 K, 48% of $[Ru(bpy)_3]^{2+*}$ excited-state underwent deactivation through the $^3$MC state, whereas this deactivation pathway remained practically unpopulated (<0.5%) in both dinuclear complexes.

## Introduction

Since the discovery of the photoluminescence of $[Ru(bpy)_3]^{2+*}$ sixty years ago,[1] the interest in its outstanding photophysical and photochemical properties has remained unaltered and ruthenium 2,2'-bipyridine type complexes have found applications in photocatalysis, artificial photosynthesis, sensing, photoelectrochemistry, nanoscale machines…[2-6] These properties include UV and visible light absorption, appreciable photoluminescence centered around 600 nm, as well as long-lived excited states with enhanced oxidizing and reducing power compared to the ground state.[7] The ground-state absorption of $[Ru(bpy)_3]^{2+}$ predominantly occurs in the high energy portion of the solar spectrum. A typical approach to increase the absorption in the visible region is to decrease the energy gap between the metal dπ and ligand-based π* acceptor orbitals through modifications of the 2,2'-bipyridine backbone.[8] This decreased energy gap leads to a bathochromic shift of the metal-to-ligand charge transfer (MLCT) absorption bands and a concomitant photoluminescence shift to lower energy.[9] Furthermore, and in accordance with the energy gap law,[10-13] the decrease in photoluminescence energy is accompanied by an increase in the direct non-radiative decay rate constant ($k_{dnr}$) and consequently a shorter excited-state lifetime (τ). An alternative approach to increase the visible light absorption is to generate polynuclear complexes, as additional metal centers are accompanied by increased molar absorption coefficients. Such Ru(II) dinuclear complexes have been reported with bridging ligands presenting two bidentate nitrogen chelating sites.[14-30] These dinuclear ruthenium(II) complexes[31] have found applications in the field of bio-imaging[32, 33], photobiology[34], photo-conversion[35, 36] and more recently in the field of photoredox catalysis.[37] Significantly, the nature of the bridging ligand is of paramount importance, as this influences the electronic communication between the metal centers, as well as the excited-state properties.[38]

In this study, the photophysical and photochemical properties of two dinuclear Ru(II) complexes (**D$_p$** and **D$_m$**) were correlated to the geometric arrangement of chelating sites of the bridging ligand, *i.e.* in the *meta* (**D$_m$**) or *para* (**D$_p$**) position with respect to the Ru(II) center anchoring site. Two regioisomers, **L$_p$** and **L$_m$**, were synthesized by homocoupling of 4- or 5-bromo-2,2'-bipyridine (**Scheme 1**). It is worth noting that both complexes were previously synthesized and electrochemically characterized, but a thorough and comprehensive investigation of their photophysical properties is still unexpectedly missing in the litterature.[39-43] Here, both complexes were characterized by UV-visible absorption spectroscopy, cyclic and differential pulsed voltammetry, as well as by steady-state and time-resolved photoluminescence over a wide temperature range. Theoretical calculations were also carried out to understand the intricacies associated with the excited-state properties of **D$_p$** and **D$_m$**. Experimental and theoretical results reported herein are compared to the prototypical $[Ru(bpy)_3]^{2+}$ and indicate that the interconnection between the two bipyridine moieties in **L$_m$** or **L$_p$** had a strikingly decisive influence on the photophysical and photochemical properties of the resulting dinuclear assembly.

[a] *Université catholique de Louvain (UCLouvain), Institut de la Matière Condensée et des Nanosciences (IMCN), Molecular Chemistry, Materials and Catalysis (MOST), Place Louis Pasteur 1, bte L4.01.02, 1348 Louvain-la-Neuve, Belgium.*
[b] *Laboratoire de Chimie Organique, Université libre de Bruxelles (ULB), CP 160/06, 50 avenue F.D. Roosevelt, 1050 Brussels, Belgium.*
[c] *Department of Chemistry, University of North Carolina at Chapel Hill, Chapel Hill, North Carolina, 27599-3290, United States.*
[d] *Département de Chimie Moléculaire, Univ. Grenoble-Alpes (UGA), UMR CNRS 5250, CS 40700, 38058 Grenoble.*
[e] *Spectroscopy, Quantum Chemistry and Atmospheric Remote Sensing (CP 160/09), Université libre de Bruxelles, 50 av. F. D. Roosevelt, B-1050 Brussels, Belgium.*
* Corresponding Author. **benjamin.elias@uclouvain.be**
Electronic Supplementary Information (ESI) available: $^1$H NMR, Mass spectrometry, Electrochemistry, Franck-Condon lineshape analysis, Variable temperature experiments, DFT calculations. See DOI: 10.1039/x0xx00000x

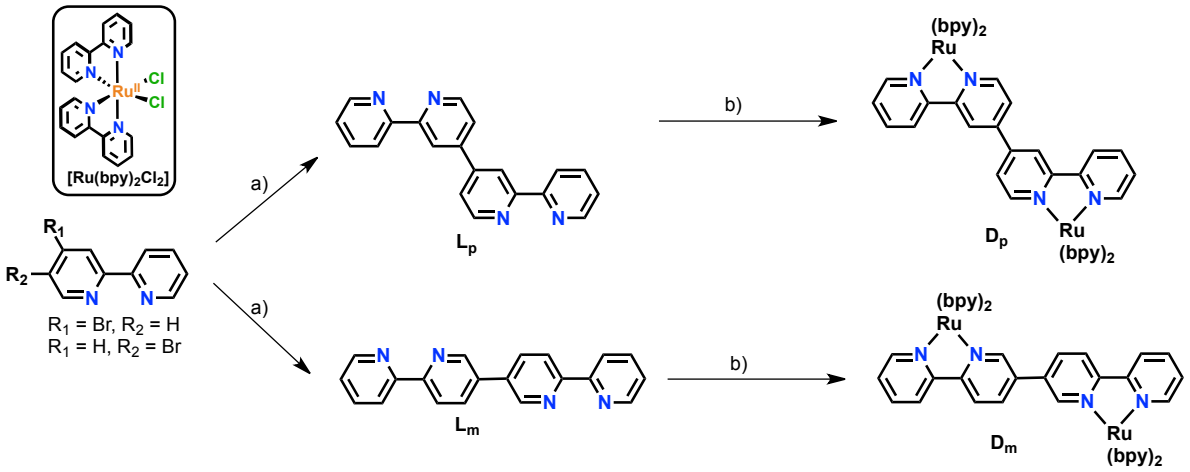


**Scheme 1.** Synthetic scheme of the desired ligands and complexes. a) $[Ni(PPh_3)_2Cl_2]$, Zn, DMF, 12h, RT, 92% (**$L_p$**), 78% (**$L_m$**) b) $[Ru(bpy)_2Cl_2]$, $AgNO_3$ $(CH_2OH)_2/H_2O$:9/1, 180 °C, MW, 1h, 77% (**$D_p$** and **$D_m$**).

## Results and discussion

The two ligands (**$L_p$**,**$L_m$**) were synthesized by a modified procedure of a previously described $Ni^0$ homo-coupling of the corresponding 4- or 5-bromo-2,2'-bipyridine (**Scheme 1**).[44] For the synthesis of the two ruthenium(II) complexes, an excess of $[Ru(bpy)_2Cl_2]$ in an ethylene glycol/water mixture was heated at 180°C in the presence of silver nitrate for 1 hour via microwave irradiation.[45] The desired dinuclear complexes (**$D_p$**,**$D_m$**) were obtained after column chromatography on silica gel and isolated as the hexafluorophosphate salts after ion metathesis. The experimental details and procedures are provided in the supplementary information.

The ground-state absorption spectra, together with the photoluminescence spectra of the three complexes are shown in **Figure 1**. A clear increase in molar absorption coefficients was observed for the dinuclear compounds. Notably, a broader, more intense $\pi \rightarrow \pi^*$ ligand-localized transition at *ca.* 280-340 nm was observed for **$D_m$** while the maxima of the lowest energy MLCT transitions remained unshifted compared to $[Ru(bpy)_3]^{2+}$. For **$D_p$**, the increase of the molar absorption coefficient for the MLCT transitions was more pronounced than that of **$D_m$** and the maxima were red-shifted by 30 nm compared to $[Ru(bpy)_3]^{2+}$.

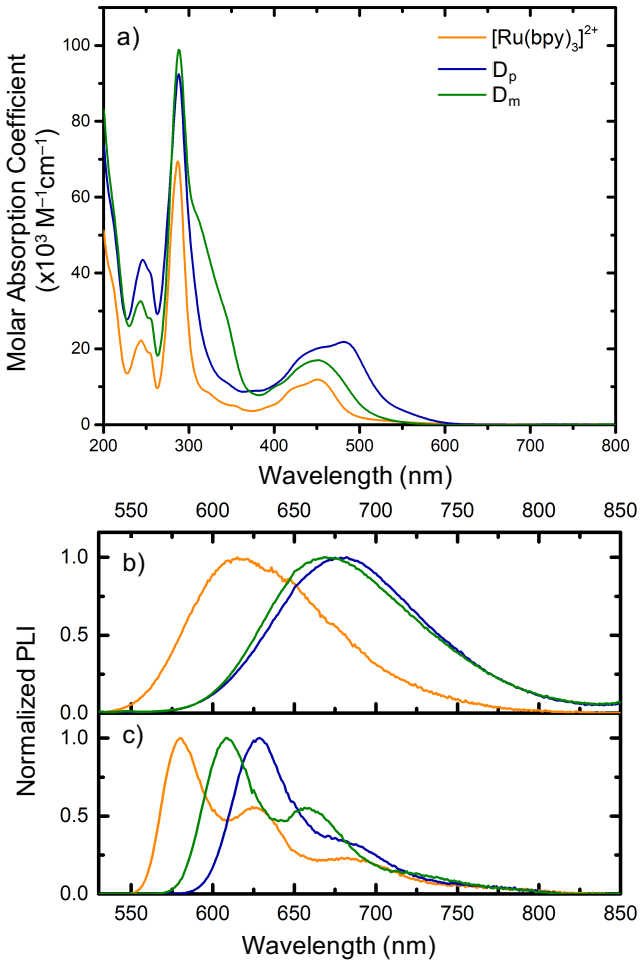


**Figure 1**. UV-Visible absorption spectra for the indicated complexes in acetonitrile at room temperature (a), normalized steady-state photoluminescence spectra of the indicated complexes in acetonitrile solution at room temperature (b) and in frozen butyronitrile matrix at 77K (c).

Hence, the interconnection of the two metallic centers through the *para* position of a bipyridine unit, *i.e.* $\mathbf{D_p}$, yielded a dinuclear complex that absorbed a broader range of the visible spectrum, with increased molar absorption coefficient.

The simulated TD-DFT absorption spectra of $\mathbf{D_p}$ and $\mathbf{D_m}$ in their ground-state singlet geometries are presented in **Figures 2a and 2c**. The heights of the excitation lines are proportional to relevant oscillator strengths (*g*). The natural transition orbitals (NTO) responsible for the strong peaks in the spectra are also displayed in **Figure 2**. The NTOs can be interpreted in a similar way as DFT orbitals, except that they are specifically adapted to the excited state of interest. TD-DFT calculations agreed with the experimental data and drew a clear picture of the transitions most likely involved upon light excitation. Indeed, the calculated absorption spectrum of $\mathbf{D_m}$ (**Figure 2c**) exhibited a relatively sharp peak in the region of 300-345 nm in addition to a broad peak between 400 and 500 nm. The transition S45, associated with the largest oscillator strength (*g* = 0.3669) for $\mathbf{D_m}$, was located at 341 nm and arose from a bridging-ligand centered excitation (LC transitions). For $\mathbf{D_p}$ (**Figure 2a**), two very broad peaks were observed in the regions of 300-340 nm and 400-550 nm, respectively, arising from many different excited states involving several orbital transitions. The largest oscillator strengths in the region of 290-340 nm were associated with transitions occurring at 299 nm (Ligand-Centered, *g* = 0.2117) (S85) and 301 nm (MLCT, *g* = 0.1796). The oscillator strengths of these transitions were lowered by as much as a factor of 2 (1.7 and 2, respectively), compared to the transitions with the largest oscillator strength of $\mathbf{D_m}$. The transition S9 at 485 nm (*g* = 0.4287) for $\mathbf{D_P}$ arose from an excited-state transition with MLCT character. A similar MLCT transition was observed for $\mathbf{D_m}$ at 483 nm (*g* = 0.1614).

At room temperature, both dinuclear complexes presented similar photoluminescence spectra that were red-shifted in comparison to $[Ru(bpy)_3]^{2+}$ (**Figure 1b**). The measured photoluminescence quantum yield (**Table 1**) of $\mathbf{D_p}$ ($\phi_{PL}$ = 0.077) was more than twice that of $\mathbf{D_m}$ ($\phi_{PL}$ = 0.034) and only slightly smaller than $[Ru(bpy)_3]^{2+}$ ($\phi_{PL}$ = 0.094). The extracted radiative rate constant, $k_r$, was larger for $\mathbf{D_m}$ ($k_r$ = 5.3 x$10^4$ $s^{-1}$) than $\mathbf{D_p}$ ($k_r$ = 3.0 x$10^4$ $s^{-1}$), and both were smaller than $[Ru(bpy)_3]^{2+}$ ($k_r$ = 11.0 x$10^4$ $s^{-1}$). The excited-state lifetime of $\mathbf{D_p}$ was surprisingly long (τ = 2.3 μs), more than twice that of $[Ru(bpy)_3]^{2+}$ (τ = 890 ns), while $\mathbf{D_m}$ had the shortest excited-state lifetime (τ = 580 ns). A more thorough examination of the deactivation rate constants (**Table 1**) allowed to gain further insights into the room temperature deactivation pathways of the excited-states. The radiative rate constant ($k_r$) of both dinuclear complexes was smaller than that of $[Ru(bpy)_3]^{2+}$ and the smallest for **Dp**. Fermi's Golden Rule indicates that the rate of radiative deactivation is proportional to the product of the cube of the energy separation between the two radiatively coupled states and the square of the transition dipole.[46-48] Nonetheless, other factors than the observed changes in energy separation induce changes in radiative rate constant. These changes can arise from variations in dipole moment or changes in the spin-orbit coupling. Changes in the spin-orbit coupling can originate from i) variations in the singlet state mixing with the triplet state, ii) variations in the energy separation between the mixed singlet and triplet states and iii) variations in the spin-orbit coupling matrix element.[49, 50, 51] The long-lived excited state of $\mathbf{D_p}$ was explained by its small non-radiative deactivation rate constant ($k_{nr}$ - four times smaller than that of $\mathbf{D_m}$). Hence, coupling two Ru(II) centers with a $\mathbf{L_p}$ or $\mathbf{L_m}$ bridging ligand increased ($\mathbf{D_m}$) or decreased ($\mathbf{D_p}$) the overall non-radiative pathways and, as a consequence, decreased or increased the excited-state luminescence lifetime compared to $[Ru(bpy)_3]^{2+}$.The photoluminescence spectra in frozen butyronitrile matrix exhibited vibronic progressions and were all blue-shifted with respect to room temperature data (**Figure 1**). Compared to $[Ru(bpy)_3]^{2+}$, the photoluminescence maxima of the two dinuclear complexes were red-shifted, with $\mathbf{D_p}$ further red-shifted by 30 nm.

The excited-state lifetime of $\mathbf{D_p}$ was almost twice as long as $\mathbf{D_m}$ in a rigid matrix at 77K, *i.e*. 9.4 μs compared to 5.2 μs respectively. At 77K, relaxation of the excited state to the ground state occurs essentially through direct radiative ($k_{dr}$) and non-radiative ($k_{dnr}$) deactivation and thermally activated deactivation processes are assumed to be negligible (*vide infra*). Franck-Condon line-shape analysis of the photoluminescence spectra recorded at 77K yielded valuable information about the excited state geometries.[13, 52-56] The emission spectra were fit according to **equation 1** where $E_0$ corresponds to the energy difference between the ground and excited-state potential energy surfaces in their $0^{th}$ vibrational level, $S_M$ is the Huang-Rhys factor, also known as the coupling factor that gauges the geometric distortion between the ground and excited state, $\hbar\omega_m$ corresponds to the vibrational energy spacings in the ground-state potential energy surface and $\Delta\nu_{1/2}$ is the full-width at half-maximum of the transition.[56, 57] The use of one vibrational mode was sufficient to fit the experimental data and no significant improvement was observed when an additional medium frequency mode was added.

$$I(\tilde{\nu}) = \sum_{\nu_m=0}^{\infty}\left[\left(\frac{E_0-\nu_m\hbar\omega_m-\nu_l\hbar\omega_l}{E_0}\right)^3 * \frac{S_M^{\nu_m}}{\nu_m!} * \exp\left\{-4\ln 2\left[\frac{\tilde{\nu}-E_0+\nu_m\hbar\omega_m}{\Delta\tilde{\nu}_{1/2}}\right]^2\right\}\right] \quad \text{Eq.1}$$

The values obtained through fits to **equation 1** are gathered in **Table 2**. The vibrational modes ($\hbar\omega_M$) were found to be of similar magnitude for all complexes, *i.e.* 1250-1260 $cm^{-1}$. These values are in good agreement with an average acceptor vibrational mode of C–C and C–N stretches in polypyridine type ligands, as already stated in literature.[55, 58, 56, 59] The $E_0$ decreased from the mononuclear to dinuclear complexes, and complex $\mathbf{D_m}$ had an $E_0$ that was 500 $cm^{-1}$ larger than $\mathbf{D_p}$, in accordance with their photoluminescence.

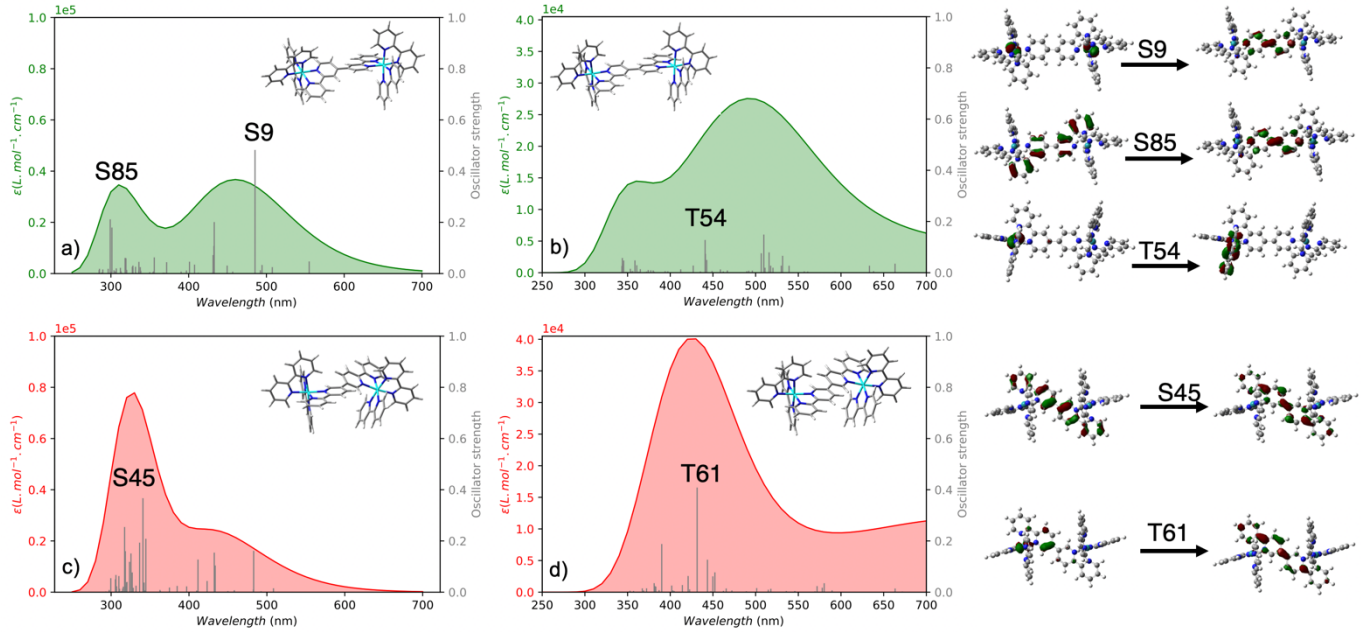


**Figure 2**. TD-DFT results used to determine the absorption properties of $\mathbf{D_P}$ (singlet-singlet (a) and triplet-triplet (b) electronic transitions) and $\mathbf{D_M}$ (singlet-singlet (c) and triplet-triplet (d) electronic transitions). The theoretical absorption spectra calculated at the ground state singlet geometries (a)-(c) and at the lowest lying triplet geometries (b)-(d) are overlaid in shaded colours. The corresponding assignments for the singlet-singlet and triplet-triplet transitions are visualized on the right.

**Table 1.** Photophysical properties of the indicated complexes.

| Complex | **Absorption** | **Photoluminescence** | | | | | | |
|---|---|---|---|---|---|---|---|---|
| | 298 K[a] | 298 K[a] | | | | | 77 K[g] | |
| | $\lambda_{max}$(nm); ε ($M^{-1}cm^{-1}$) | $\lambda_{max}$ (nm)[b] | τ (ns)[c] | $\Phi_{PL}$[d] | $k_r$ ($10^4$ $s^{-1}$)[e] | $k_{nr}$ ($10^6$ $s^{-1}$)[f] | $\lambda_{max}$ (nm) | τ (μs) |
| $\mathbf{D_p}$ | (288; 92,500), (481; 21,800) | 682 | 2350 (280) | 0.077 (0.010) | 3.0 | 0.4 | 629 | 9.4 |
| $\mathbf{D_m}$ | (288; 98,900), (330; 38,800), (451; 17,000) | 670 | 580 (220) | 0.034 (0.013) | 5.3 | 1.7 | 610 | 5.2 |
| $[Ru(bpy)_3]^{2+}$ | (287; 69,400), (450; 12,000) | 615 | 890 (170) | 0.094 (0.018) | 11.0 | 1.0 | 579 | 4.8 |

[a] acetonitrile solution. [b] excitation at 450 nm. [c] in argon purged acetonitrile solution with values for air-equilibrated solution in parenthesis. Uncertainties are estimated to be 2%. [d] in argon purged acetonitrile solution with $[Ru(bpy)_3]^{2+}$ in air-equilibrated acetonitrile used as reference ($\Phi_{PL}$=0.018).[60] Uncertainties are estimated to be 10%. [e] $k_r = \Phi_{PL}/\tau$. [f] $\tau = 1/(k_r+k_{nr})$. [g] Butyronitrile rigid matrix.

**Table 2.** Fitting parameters obtained from the Franck-Condon lineshape analysis[a]

| Complex | $E_0$ ($cm^{-1}$) | $\hbar\omega_M$ ($cm^{-1}$) | $S_M$ | fwhm ($cm^{-1}$) |
|---|---|---|---|---|
| $\mathbf{D_p}$ | 15900 | 1250 | 0.46 | 1020 |
| $\mathbf{D_m}$ | 16400 | 1260 | 0.71 | 990 |
| $[Ru(bpy)_3]^{2+}$ | 17180 | 1250 | 0.82 | 940 |

[a] At 77 K in butyronitrile rigid matrix, no parameters were constrained for the fit.

The Huang-Rhys factor, $S_M$, displayed the most significant difference. Only a small decrease was observed from $[Ru(bpy)_3]^{2+}$ to $\mathbf{D_m}$ (0.82 to 0.71), while $\mathbf{D_p}$ exhibited a more pronounced decrease (0.41). A smaller value of $S_M$ is indicative of less distorted excited state compared to the ground state. This is usually attributed to efficient electron delocalization over the whole accepting ligand where only small changes in the C–C and C–N bond are observed.[55, 61, 62] In other words, the geometry of the bridging ligand resulted in a more delocalized excited state in $\mathbf{D_p}$ than in $\mathbf{D_m}$. Calculated NTOs and the spatial extent $<R^2>$ values calculated by Gaussian from the DFT densities provided complimentary information that agreed with the experimental observations. NTOs identified the atoms and bonds over which the electronic transition density matrices were distributed while $<R^2>$ values provided information about the radial extent of the electronic distribution. The $<R^2>$ value for the lowest-lying triplet geometry of $\mathbf{D_p}$ was 20% larger than the one obtained for the lowest-lying triplet geometry of $\mathbf{D_m}$, *i.e.* 85450 a.u. and 71719 a.u., respectively. The longer excited-state lifetime of $\mathbf{D_p}$ compared to $\mathbf{D_m}$ also agreed with the difference in the Huang-Rhys factors. The more extended excited-state delocalization of $\mathbf{D_p}$ decreased the direct non-radiative deactivation ($k_{dnr}$) to the ground state and, consequently, increased the overall excited-state lifetime.[46, 49, 61]

Nanosecond transient absorption spectra of the dinuclear complexes in butyronitrile at 298K are presented in **Figure 3**.

Transient absorption spectroscopy revealed two distinct excited-state behaviors. For $\mathbf{D_p}$ and $\mathbf{D_m}$, the transient absorption changes decayed according to a unimolecular process over the whole spectral range on a timescale consistent with time-resolved photoluminescence measurements. This was consistent with excited-state relaxation occurring from the $^3$MLCT excited-state.[63] The transient spectra of $\mathbf{D_p}$ were similar to those of $[Ru(bpy)_3]^{2+}$,[64] where an MLCT bleach was observed between 400 and 520 nm, consistent with formal oxidation of Ru(II) to Ru(III). The positive transient absorption features between 520 and 800 nm were attributed to intra-ligand transitions of the formally monoreduced $\mathbf{L_p}^{\bullet-}$ radical anion.[65] With $\mathbf{D_m}$, the MLCT bleach associated to the oxidation of Ru(II) to Ru(III) was hidden by the positive transient absorption features involving the monoreduced $\mathbf{L_m}^{\bullet-}$ radical anion. Indeed, hints of the fundamental bleach were observed around 490 nm.[41] The prototypical $[Ru(bpy)_3]^{2+}$ excited-state is characterized by additional transient absorption changes around 370 nm (not shown here).[63, 66, 67] These absorption changes are also attributed to transitions localized on the reduced bipyridine ligand.[68, 69] Here, it was proposed that a similar bridging ligand-centered transitions occurred within $\mathbf{D_m}$, but were shifted towards lower energy and therefore also overlapping with the fundamental MLCT bleach. This was consistent with the broader ground state $\pi\rightarrow\pi^*$ ligand-localized transition observed for $\mathbf{D_m}$ that absorbed light up to 370 nm (compared to 310 nm for $\mathbf{D_p}$ or $[Ru(bpy)_3]^{2+}$).

Additionally, in linear poly(*p*-phenylene) radical anions, an increase of phenyl units is accompanied by a bathochromic shift of the high energy transition. Hence, a similar trend could be observed for $\mathbf{L_m}$.[70]

Further information was garnered by TD-DFT calculations. The simulated TD-DFT absorption spectra of $\mathbf{D_p}$ and $\mathbf{D_m}$ in their lowest-lying triplet geometries (corresponding to the light-induced excited-states) with the natural transition orbitals (NTO) responsible for the strong peaks in the spectra, are presented in **Figures 2b and 2d**. As for the GS analysis (*vide supra*), TD-DFT calculations were in good agreement with the experimental measurements. Indeed, the calculated absorption spectrum for $\mathbf{D_m}$ exhibited a sharp peak around 430 nm. A main transition (T61) was associated with a very large oscillator strength, *i.e.* 0.4084 at 432 nm. This transition agreed with a mixed metal-ligand-to-ligand charge transfer (MLLCT), as electron density was initially present on both a portion of $\mathbf{L_m}$ and one Ru center and was then transferred to $\mathbf{L_m}$. For $\mathbf{D_p}$, the transitions associated with the largest oscillator strength were found at 440 nm ($g$ = 0.1277) (T54) and 510 nm ($g$ = 0.1488) (T35) showing that transitions from the triplet state of $\mathbf{D_m}$ around 430 nm were twice as intense as the one associated with the triplet state of $\mathbf{D_p}$.

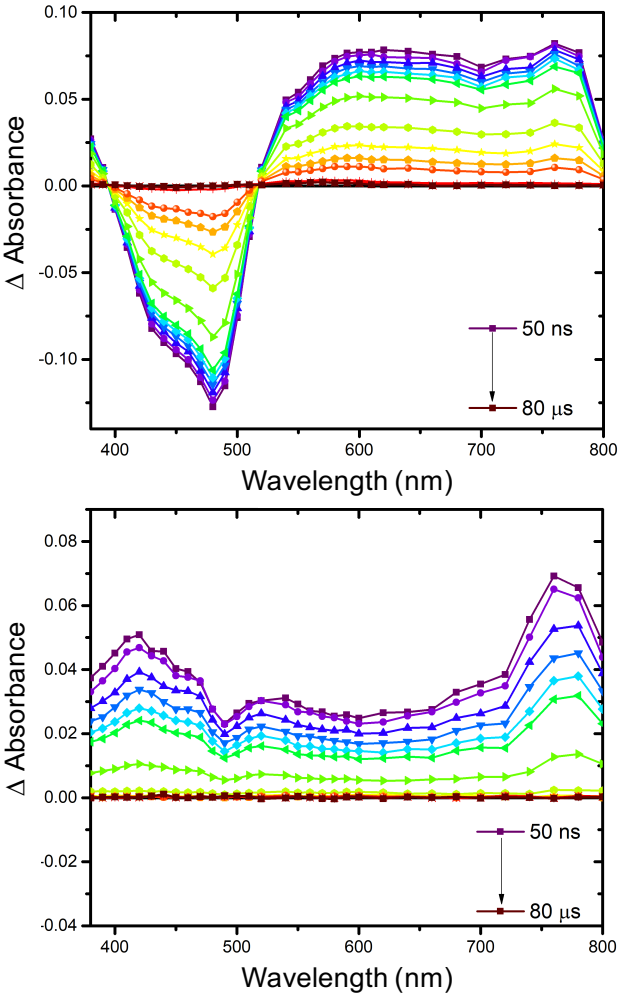


**Figure 3**. Transient absorption spectra at 298K of $\mathbf{D_p}$ (top) and $\mathbf{D_m}$ (bottom) after pulsed 532 nm light excitation in argon purged butyronitrile.

**Variable temperature experiments.**

Variable temperature photoluminescence measurements were carried out in an effort to gain insight into the processes involved in the excited-state deactivation pathways, hence providing photophysical schemes for $\mathbf{D_p}$ and $\mathbf{D_m}$ and subsequent quantification of the associated deactivation rate constants. The photophysical scheme of the prototypical $[Ru(bpy)_3]^{2+}$ is well established with a thermally equilibrated excited state that in fact corresponds to three closely lying triplet metal-to-ligand-charge-transfer ($^3$MLCT) excited states.[71, 72] In addition to direct radiative and non-radiative decay to the ground state, these $^3$MLCT excited states can deactivate via thermally activated processes, *i.e.* through population of an upper lying metal-centered state ($^3$MC) or through population of a fourth $^3$MLCT.[73, 74]

The temperature dependence of the excited-state lifetimes and steady-state photoluminescence spectra was studied in butyronitrile solution. Changes in the photoluminescence spectra of $\mathbf{D_p}$ and $\mathbf{D_m}$ are represented in **Figure 4**. Overall, the excited-state lifetimes and absolute photoluminescence quantum yields decreased with a temperature increase (**Figure 4 c** and **f)**. Nevertheless, the two dinuclear complexes displayed

significantly different behavior upon temperature changes. Characteristic behavior, reminiscent of $[Ru(bpy)_3]^{2+}$, was observed for $\mathbf{D_m}$, where a slight redshift of the photoluminescence maximum was observed as the temperature increased. In the case of $\mathbf{D_p}$, a blue-shift and broadening of the photoluminescence was observed as the temperature increased.

The changes in the excited-state lifetimes ($\tau$) with temperature were fit using **equation 2**,[75, 76] where $k_{dr}$ and $k_{dnr}$ are the activationless direct radiative and nonradiative decay rate constants of the three closely spaced thermally equilibrated $^3$MLCTs back to the ground state, considered to remain constant within the range of temperatures studied.

$$1/\tau = k_{dr} + k_{dnr} + k_{3MC} + k_{3MLCT} = k_{dr} + k_{dnr} + A_{3MC}e^{-E_{3MC}/RT} + A_{3MLCT}e^{-E_{3MLCT}/RT} \quad \text{Eq. 2}$$

$k_{3MC}$ and $k_{3MLCT}$ are the temperature dependent deactivation rate constants associated with the thermal population of the $^3$MC state or 4$^{th}$ $^3$MLCT, respectively. These deactivation pathways were characterized by the pre-exponential factors $A_{3MC}$ and $A_{3MLCT}$, as well as the corresponding activation energies, $E_{3MC}$ and $E_{3MLCT}$. The photoluminescence decays were considered as mono-exponential at all temperatures investigated. The parameters abstracted from **equation 2** are gathered in **Table 3**.

Both dinuclear complexes and $[Ru(bpy)_3]^{2+}$ displayed two thermally activated deactivation pathways.[74, 77] The first one ($k_{3MC}$) was attributed to the population of the metal-centered ($^3$MC) excited-state (also called ligand-field state) with higher activation energy ($E_{3MC}$ > 3000 cm$^{-1}$) and larger pre-exponential factor ($A_{3MC}$ $10^{12}$-$10^{14}$ s$^{-1}$). [8, 9, 72, 74, 75, 78, 79] The second one ($k_{3MLCT}$) was associated with lower activation energy ($E_{3MLCT}$ ~ 300-1000 cm$^{-1}$), smaller pre-exponential factor ($A_{3MLCT}$ ~$10^6$ s$^{-1}$), and attributed to the relaxation through an upper lying $^3$MLCT excited-state.[73, 78, 80] The lowest $^3$MLCT excited state is coupled with the upper lying $^3$MLCT excited state ($^3MLCT_{lowest} \leftrightarrow {}^3MLCT_{upper}$) and the energy gap between these two states is given by $E_{3MLCT}$. The deactivation rate constant of the upper lying $^3$MLCT excited state ($A_{3MLCT}$) is the sum of the radiative and non-radiative decay rate constant from this state to the ground state.[73, 79]

The direct radiative ($k_{dr}$) and non-radiative ($k_{dnr}$) deactivation from the three closely lying $^3$MLCT excited-states increased by a factor of two from $\mathbf{D_p}$ to $\mathbf{D_m}$. As mentioned above, this can be rationalized by a more delocalized excited state in $\mathbf{D_p}$, as evidenced by the smaller Huang-Rhys factor, decreasing the rate of the direct non-radiative deactivation ($k_{dnr}$). Thermal deactivation from the three closely lying $^3$MLCT excited states first occurred via the upper-lying 4$^{th}$ MLCT excited-state and, at higher temperature, an additional deactivation pathway via the $^3$MC was operative (**Figure 5**). Both $k_{3MC}$ and $k_{3MLCT}$ were significantly enhanced in $\mathbf{D_m}$ compared to $\mathbf{D_p}$. As a consequence, the shorter excited-state lifetime of $\mathbf{D_m}$ was attributed to increased rates of the direct ($k_{dr}$, $k_{dnr}$) and activated ($k_{3MC}$, $k_{3MLCT}$) deactivation, which clearly underlined the crucial role played by the geometry of the bridging ligand in the excited-state deactivation pathways (**Figure 6**).

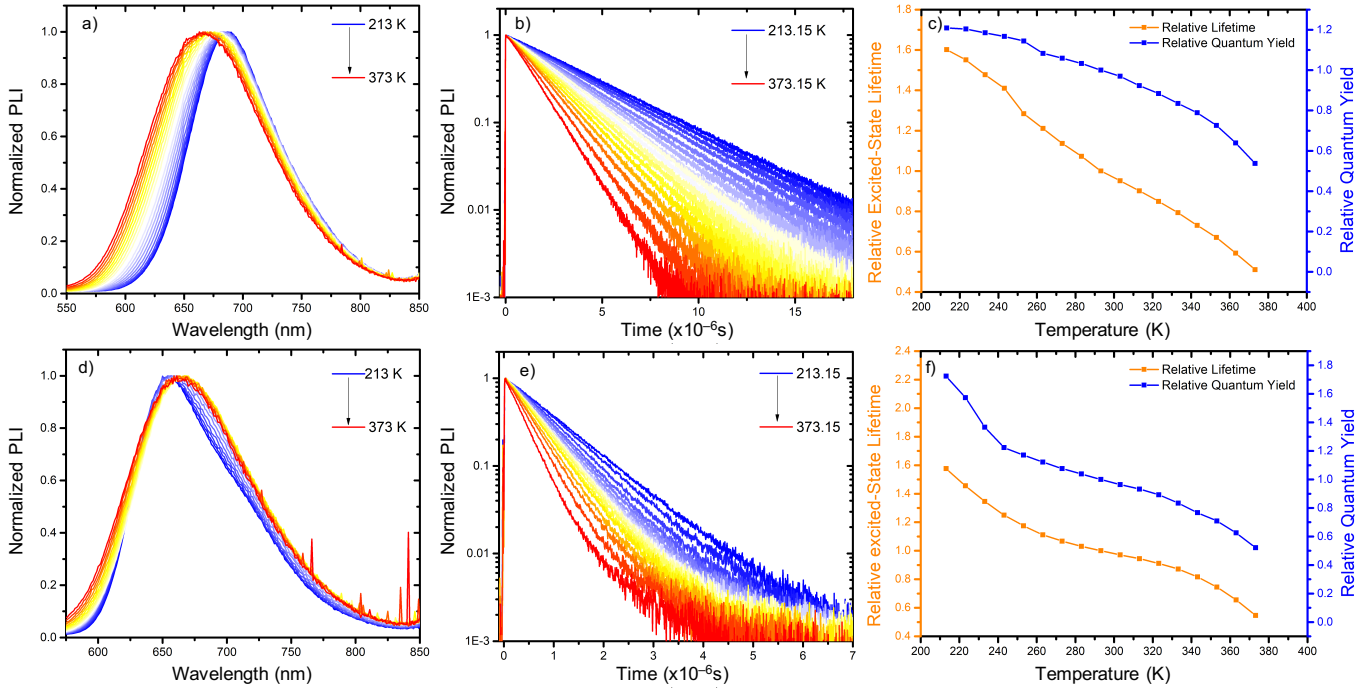


**Figure 4.** Normalized steady-state and time-resolved photoluminescence, as well as the relative excited-state lifetimes (orange) and photoluminescence quantum yields (blue) of $\mathbf{D_p}$ (a-c) and $\mathbf{D_m}$ (d-f) in argon purged butyronitrile.

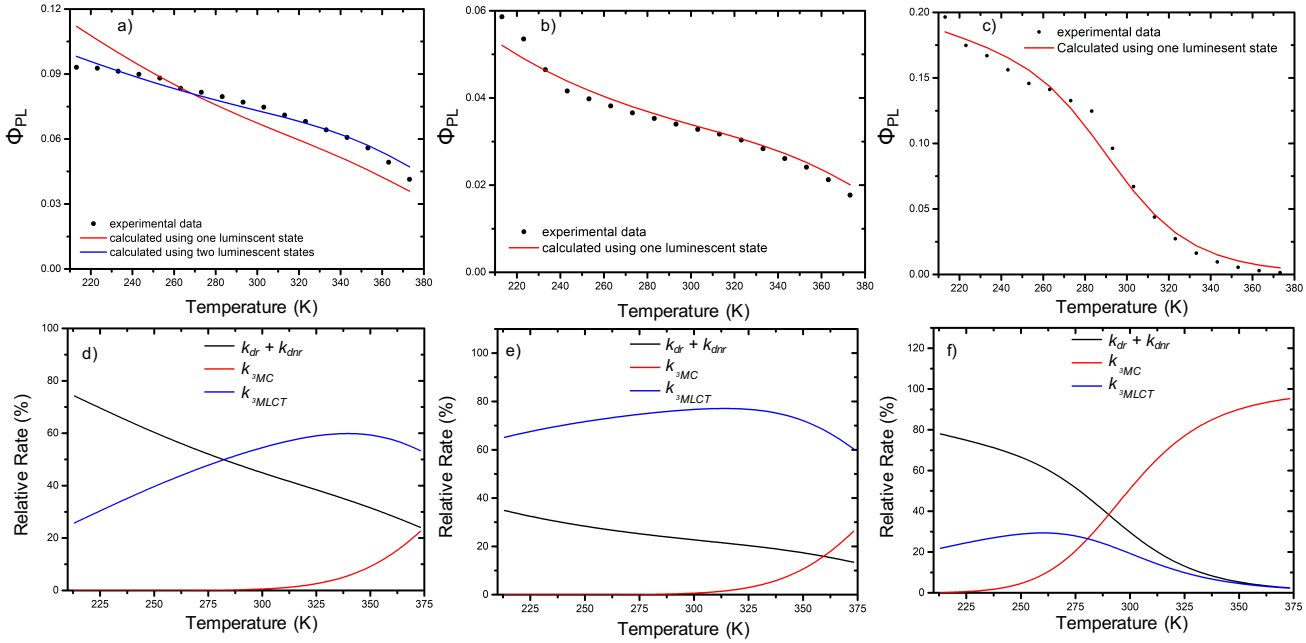


**Figure 5**. Measured and calculated quantum yields of $\mathbf{D_p}$ (a), $\mathbf{D_m}$ (b) and $[Ru(bpy)_3]^{2+}$ (c) as a function of temperature. The black dots represent the experimentally determined quantum yields at various temperatures. The red line represents the calculated quantum yields if only the lowest $^3$MLCT excited state is luminescent. The blue line represents the calculated quantum yields if the lowest and the thermally activated $^3$MLCT excited state are luminescent. Relative rates of deactivation of the lowest $^3$MLCT excited state of $\mathbf{D_p}$ (d), $\mathbf{D_m}$ (e) and $[Ru(bpy)_3]^{2+}$ (f) via different pathway. (Black) direct radiative and nonradiative deactivation to the ground state, (blue) thermally activated deactivation through the upper lying $^3$MLCT excited state and (red) thermally activated deactivation through the $^3$MC excited state

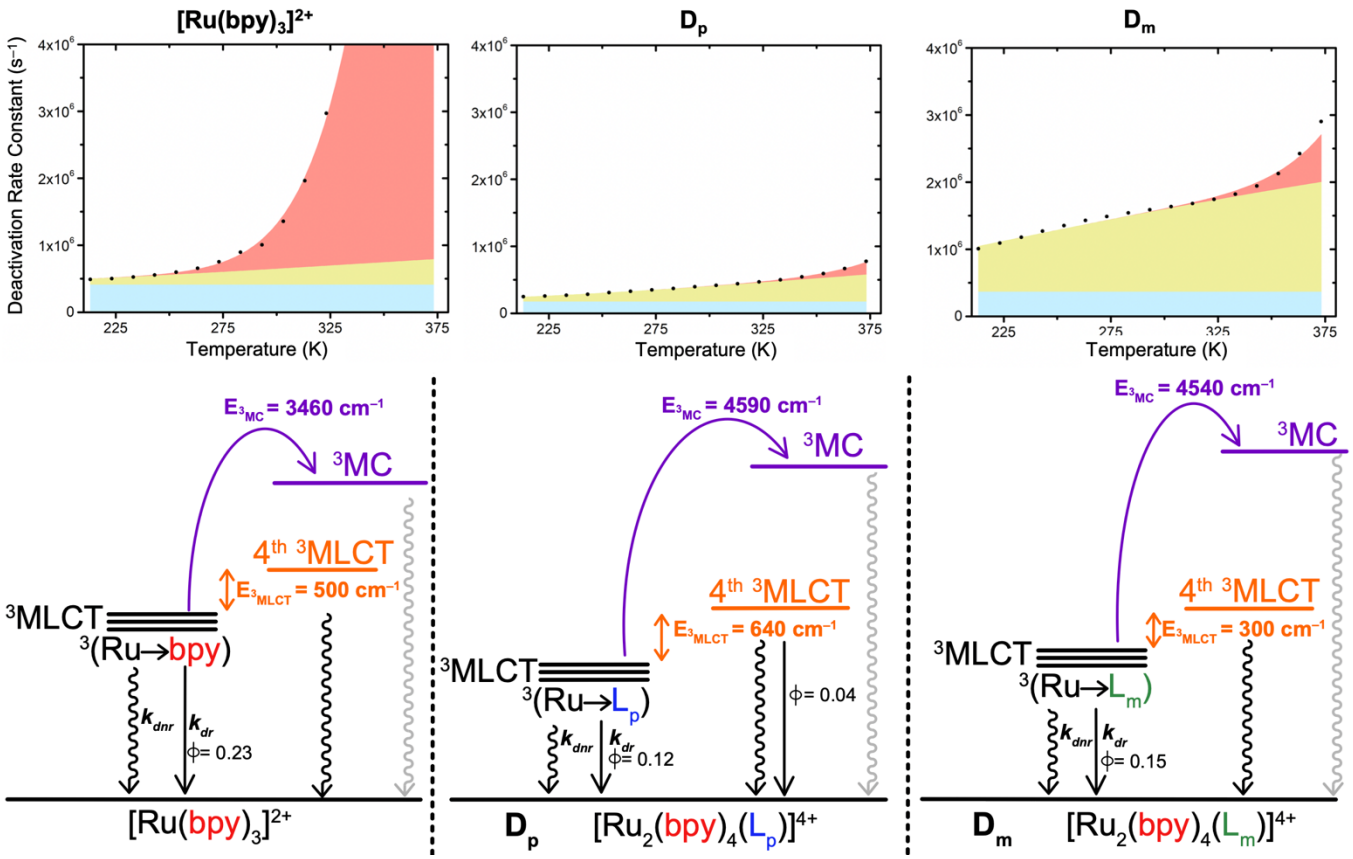


**Figure 6.** (Above) Excited-state deactivation rate constants for complexes $[Ru(bpy)_3]^{2+}$, $\mathbf{D_p}$ and $\mathbf{D_m}$. (Blue) direct radiative and nonradiative rate constants ($k_{dr} + k_{nr}$), (yellow) thermally activated deactivation via the upper lying $^3$MLCT ($k_{^3MLCT}$), (red) thermally activated deactivation via the upper lying $^3$MC ($k_{^3MC}$) and (dot) experimental data. (Below) Proposed photophysical schemes for $[Ru(bpy)_3]^{2+}$, $\mathbf{D_p}$ and $\mathbf{D_m}$.

Table 3. Kinetic parameters for the excited-state decay in butyronitrile solution

| Complex | $k_{dr} + k_{dnr}$ ($s^{-1}$) | $A_{3MC}$ ($s^{-1}$) | $E_{3MC}$ ($cm^{-1}$) | $A_{3MLCT}$ ($s^{-1}$) | $E_{3MLCT}$ ($cm^{-1}$) | $\Phi_{PL}$ $^3$MLCT ($k_{dr}/k_{dr}+k_{dnr}$) | $\Phi_{PL}$ $^3$MLCT (thermally activated) ($A_{3MLCT\ radiative}/A_{3MLCT}$) |
|---|---|---|---|---|---|---|---|
| $\mathbf{D_p}$ | $1.8x10^5$ | $8.5x10^{12}$ | 4590 | $4.8x10^6$ | 640 | 0.12 ± 0.01 | 0.04 ± 0.01 |
| $\mathbf{D_m}$ | $3.6x10^5$ | $2.8x10^{13}$ | 4540 | $5.3x10^6$ | 300 | 0.15 ± 0.01 | ---[a] |
| $[Ru(bpy)_3]^{2+}$ | $4.1x10^5$ | $1.1x10^{13}$ | 3460 | $2.6x10^6$ | 500 | 0.23 ± 0.01 | ---[a] |

[a] The close match between the calculated and measured quantum yields suggested that the deactivation pathway through the thermally activated $^3$MLCT (upper lying) excited-state was non-luminescent or too weak to be detected.

For $[Ru(bpy)_3]^{2+}$, the deactivation first occurred through the upper lying $^3$MLCT ($k_{3MLCT}$) followed by an irreversible population of the $^3$MC ($k_{3MC}$).[54, 81] However, due to its low activation energy barrier (3460 $cm^{-1}$), deactivation via the $^3$MC state ($k_{3MC}$) started to contribute significantly at 80 degrees lower than for the two dinuclear complexes. Strikingly, at 298 K, 48% of the excited-state deactivation occurred through population of the $^3$MC, in comparison to only 0.5% for either dinuclear complex (**Figure 6**). It was however not possible to determine whether the population of the $^3$MC was a reversible or irreversible process for the dinuclear complexes.[79] The thermal population of the $^3$MC excited-state led predominantly to non-radiative deactivation back to the ground state, but also to ligand-loss.[82, 83] As a consequence, a smaller population of the $^3$MC induced a much higher photostability for both dinuclear complexes compared to $[Ru(bpy)_3]^{2+}$.[75, 84]

**Photophysical schemes and PL quantum yields of the 4$^{th}$ $^3$MLCT**

The information gathered in this study have allowed to propose photophysical schemes for the three complexes (**Figure 6**). For $\mathbf{D_m}$, the $^1$MLCT transitions from the Ru(II) to the 2,2'-bipyridine or the bridging ligand ($\mathbf{L_m}$) occurred at similar energies. Consequently, its absorption spectrum was similar to that of $[Ru(bpy)_3]^{2+}$, where $^1$MLCT transitions only occur from the Ru(II) to 2,2'-bipyridines. In the case of $\mathbf{D_p}$, the $^1$MLCT transition from Ru(II) to the bridging ligand ($\mathbf{L_p}$) occurred at a significantly lower energy than the transitions to the 2,2'-bipyridines. This allowed these two transitions to be distinguished in the visible part of the absorption spectrum. In both dinuclear complexes, the photoluminescence originated from $^3$MLCT excited states and spectroelectrochemical correlation[9] suggested that the excited-state formation corresponded to a charge transfer from the ruthenium(II) center to the bridging ligand.

The activationless direct radiative rate constant ($k_{dr}$) was determined by a fit of the measured photoluminescence quantum yields at various temperatures using **Equation 3**.[76] The parameters that were determined ($k_{dr} + k_{dnr}$, $A_{3MLCT}$, $E_{3MLCT}$, $A_{3MC}$ and $E_{3MC}$) are gathered in **Table 3**. The photoluminescence quantum yield from the lowest $^3$MLCT excited state was determined though the relationship: ($k_{dr}$ / $k_{dr}$ + $k_{dnr}$).

$$\phi(T) = \frac{k_{dr}}{k_{dr}+k_{dnr}+A_{3MLCT}e^{-E_{3MLCT}/RT}+A_{3MC}e^{-E_{3MC}/RT}} \quad \text{Eq. 3}$$

$$\phi(T) = \frac{k_{dr}+A_{3MLCT\ radiative}e^{-E_{3MLCT}/RT}}{k_{dr}+k_{dnr}+A_{3MLCT}e^{-E_{3MLCT}/RT}+A_{3MC}e^{-E_{3MC}/RT}} \quad \text{Eq. 4}$$

For $\mathbf{D_m}$ and $[Ru(bpy)_3]^{2+}$, close matches between the calculated and experimentally determined quantum yields were obtained using **Equation 3** (**Figure 5b-c**), which implied that the deactivation pathway through the thermally activated $^3$MLCT (upper lying) excited-state was non-luminescent or too weak to be detected. This was also underlined by the proportional evolution observed between the relative excited-state lifetime and relative quantum yield of photoluminescence for $\mathbf{D_m}$ (**Figure 4f**). Hence, for $\mathbf{D_m}$ and $[Ru(bpy)_3]^{2+}$, only the lowest $^3$MLCT were subject to radiative deactivation and both deactivation pathways via the $^3$MC and the upper-lying $^3$MLCT were non-radiative. The decreased photoluminescence intensity and lifetime with temperature were attributed to increased deactivation via the $^3$MC and the upper lying $^3$MLCT excited-states, both being non-luminescent states. In the case of $\mathbf{D_p}$, the blue-shift of the photoluminescence with increased temperature was explained by the thermal population ($k_{3MLCT}$) of the upper-lying $^3$MLCT excited-state, which luminesces at higher energy.[85-87] Indeed, a close match between the calculated and experimentally measured quantum yields could only be obtained when an additional radiative deactivation pathway from the thermally activated $^3$MLCT excited state to the ground state was considered (**Figure 5a**). This behaviour was also supported by the non-proportional evolution observed between the relative excited-state lifetime and relative quantum yield of photoluminescence for $\mathbf{D_p}$ (**Figure 4c**). In this case, the photoluminescence quantum yields as a function of temperature were fit using **Equation 4**, where $A_{3MLCT\ radiative}$ is the radiative deactivation rate constant of the upper lying $^3$MLCT excited state to the ground state. The photoluminescence quantum yield of the upper lying $^3$MLCT excited-state was determined using the relationship: ($A_{3MLCT\ radiative}$ / $A_{3MLCT}$). As evidenced, the proportion of radiative deactivation from the upper lying $^3$MLCT over the lower $^3$MLCT increased with temperature and resulted in a blue shift of the photoluminescence maxima. Such behavior has already been observed for ruthenium(II) 2,2'-biquinoline and dipyrido[3,2-c:2',3'-e]pyridazine complexes,[85, 87] $[Ru(bpy)_3]^{2+}$ in KBr disc[74] and Ru(II) bipyridine complexes with conjugated thiophene substituents[88] and osmium(II) bis-terpyridine complexes.[51]

The constant and unimolecular behavior of the luminescent excited-state lifetime at different wavelengths was consistent with dual emission, originating from two equilibrated luminescent excited states for $\mathbf{D_p}$.[76, 78, 88-91] Hence, only the $^3$MC was non-luminescent in $\mathbf{D_p}$. A combination of the photoluminescence quantum yields and the population of the

different excited states as a function of temperature (**Figure 4-6**) yielded an estimate of the photoluminescence quantum yields of the two different $^3$MLCT excited states (**Figure 6** and **Table 3**).[76]

## Conclusions

The change from mononuclear $[Ru(bpy)_3]^{2+}$ to dinuclear complexes $\mathbf{D_p}$ and $\mathbf{D_m}$ was accompanied by a bathochromic shift of the photoluminescence and a drastic decrease of the thermal population of the $^3$MC excited-state. At room temperature, deactivation from the $^3$MC was virtually absent for $\mathbf{D_p}$ and $\mathbf{D_m}$, whereas 48% of $[Ru(bpy)_3]^{2+}$ excited-state was deactivated through that state. The prime advantage of controlling the population of the $^3$MC excited-state is to limit or inhibit the ligand-loss often associated with this state, hence reducing deactivation via a non-radiative pathway. This bears immediate consequence for research in bio-imaging[32, 33], photobiology[34], photo-conversion[35, 36], as well as photoredox catalysis.[37]

A drastic influence of the geometry of the connection between the two bipyridine parts of the bridging ligand was shown. Connection through the *para* position of the 2,2'-bipyridine, as in complex $\mathbf{D_P}$, increased the portion of absorbed visible light, as well as the molar absorption coefficient, and decreased the rate constants of direct ($k_{dr}$ + $k_{dnr}$) and activated deactivation pathways ($k_{3MC}$ + $k_{3MLCT}$). By comparison, only the molar absorption coefficient was increased for $\mathbf{D_m}$, *i.e*. when the two 2,2'-bipyridine were connected in the *meta* position, while the deactivation rate constants all increased. Consequently, at room temperature the excited state lifetimes followed the trend $\mathbf{D_p}$ (2.35 µs) >> $[Ru(bpy)_3]^{2+}$ (890 ns) > $\mathbf{D_m}$ (580 ns).

Variable temperature measurements allowed the determination of the activation energies for crossing to the $^3$MC state and the fourth, upper lying, $^3$MLCT state. This higher energy $^3$MLCT was populated in the three ruthenium(II) complexes but only $\mathbf{D_p}$ exhibited photoluminescence from that state, while for $[Ru(bpy)_3]^{2+}$ and $\mathbf{D_m}$ it was deactivated solely through non-radiative processes. For $\mathbf{D_p}$, the smallest rate constants for the nonradiative pathway and the presence of two luminescent $^3$MLCT states resulted in a photoluminescence quantum yield more than twice that of $\mathbf{D_m}$ and only slightly smaller than $[Ru(bpy)_3]^{2+}$. It was proposed that the more delocalized excited state of $\mathbf{D_p}$, as evidenced by the small Huang-Rhys factor, was responsible for the smaller non-radiative deactivation rate constants in comparison to $\mathbf{D_m}$.

## Conflicts of interest

There are no conflicts to declare.

## Acknowledgements

L.T.-G. acknowledges the F.R.S.-FNRS for his "Chargé de Recherches" fellowship. S.C. and B.E. gratefully acknowledge the UCLouvain for financial support. The authors acknowledge Gerald J. Meyer for the scientific generosity and providing access to his equipment. Steady-State and time-resolved absorption and photoluminescence experiments were performed using instrumentation in the Alliance for Molecular PhotoElectrode Design for Solar Fuels (AMPED), an Energy Frontier Research Center (EFRC) funded by the U.S. Department of Energy (DOE), Office of Science, Basic Energy Sciences BES, under Award DE-SC0001011. Computational resources have been provided by the Shared ICT Services Centre, Université Libre de Bruxelles." The NanoBio-ICMG platform (FR 2607) is greatly acknowledged.

## Notes and references

1. J. P. Paris and W. W. Brandt, *J. Am. Chem. Soc.*, 1959, **81**, 5001-5002.
2. S. Campagna, F. Puntoriero, F. Nastasi, G. Bergamini and V. Balzani, in *Photochemistry and Photophysics of Coordination Compounds I*, ed. S. C. Vincenzo Balzani, Springer, Berlin, Heidelberg, 2007, vol. 280, pp. 117-214.
3. J. Larsen, F. Puntoriero, T. Pascher, N. McClenaghan, S. Campagna, E. Åkesson and V. Sundström, *ChemPhysChem*, 2007, **8**, 2643-2651.
4. L. Troian-Gautier, M. D. Turlington, S. A. M. Wehlin, A. B. Maurer, M. D. Brady, W. B. Swords and G. J. Meyer, *Chem. Rev.*, 2019, **119**, 4628-4683.
5. L. Troian-Gautier and C. Moucheron, *Molecules*, 2014, **19**.
6. C. K. Prier, D. A. Rankic and D. W. C. MacMillan, *Chem. Rev.*, 2013, **113**, 5322-5363.
7. R. J. Watts, *J. Chem. Educ.*, 1983, **60**, 834.
8. A. Juris, V. Balzani, F. Barigelletti, S. Campagna, P. Belser and A. von Zelewsky, *Coord. Chem. Rev.*, 1988, **84**, 85-277.
9. F. Barigelletti, A. Juris, V. Balzani, P. Belser and A. Von Zelewsky, *Inorg. Chem.*, 1987, **26**, 4115-4119.
10. J. V. Caspar and T. J. Meyer, *J. Phys. Chem.*, 1983, **87**, 952-957.
11. K. R. Barqawi, Z. Murtaza and T. J. Meyer, *J. Phys. Chem.*, 1991, **95**, 47-50.
12. J. A. Treadway, B. Loeb, R. Lopez, P. A. Anderson, F. R. Keene and T. J. Meyer, *Inorg. Chem.*, 1996, **35**, 2242-2246.
13. E. M. Kober, J. V. Caspar, R. S. Lumpkin and T. J. Meyer, *J. Phys. Chem.*, 1986, **90**, 3722-3734.
14. J. Bolger, A. Gourdon, E. Ishow and J.-P. Launay, *Inorg. Chem.*, 1996, **35**, 2937-2944.
15. A. Kirsch-De Mesmaeker, L. Jacquet, A. Masschelein, F. Vanhecke and K. Heremans, *Inorg. Chem.*, 1989, **28**, 2465-2470.
16. A. Boisdenghien, C. Moucheron and A. Kirsch-De Mesmaeker, *Inorg. Chem.*, 2005, **44**, 7678-7685.
17. B. Elias, L. Herman, C. Moucheron and A. Kirsch-De Mesmaeker, *Inorg. Chem.*, 2007, **46**, 4979-4988.
18. M.-J. Kim, R. Konduri, H. Ye, F. M. MacDonnell, F. Puntoriero, S. Serroni, S. Campagna, T. Holder, G. Kinsel and K. Rajeshwar, *Inorg. Chem.*, 2002, **41**, 2471-2476.
19. Y. Fuchs, S. Lofters, T. Dieter, W. Shi, R. Morgan, T. C. Strekas, H. D. Gafney and A. D. Baker, *J. Am. Chem. Soc.*, 1987, **109**, 2691-2697.
20. S. Kohlmann, S. Ernst and W. Kaim, *Angewandte Chemie International Edition in English*, 1985, **24**, 684-685.
21. G. S. Hanan, C. R. Arana, J.-M. Lehn and D. Fenske, *Angewandte Chemie International Edition in English*, 1995, **34**, 1122-1124.

22. F. Loiseau, F. Nastasi, A.-M. Stadler, S. Campagna and J.-M. Lehn, *Angew. Chem. Int. Ed.*, 2007, **46**, 6144-6147.
23. K. Kalyanasundaram and M. K. Nazeeruddin, *Inorg. Chem.*, 1990, **29**, 1888-1897.
24. F. Masaoki, K. Noritaka and N. Shun-ichi, *Chem. Lett.*, 1986, **15**, 1209-1212.
25. G. F. Strouse, J. R. Schoonover, R. Duesing, S. Boyde, W. E. Jones, Jr. and T. J. Meyer, *Inorg. Chem.*, 1995, **34**, 473-487.
26. L. De Cola, V. Balzani, F. Barigelletti, L. Flamigni, P. Belser, A. von Zelewsky, M. Frank and F. Voegtle, *Inorg. Chem.*, 1993, **32**, 5228-5238.
27. A. I. Baba, H. E. Ensley and R. H. Schmehl, *Inorg. Chem.*, 1995, **34**, 1198-1207.
28. M. Frank, M. Nieger, F. Vögtle, P. Belser, A. von Zelewsky, L. De Cola, V. Balzani, F. Barigelletti and L. Flamigni, *Inorg. Chim. Acta.*, 1996, **242**, 281-291.
29. V. Balzani, F. Barigelletti, P. Belser, S. Bernhard, L. De Cola and L. Flamigni, *J. Phys. Chem.*, 1996, **100**, 16786-16788.
30. K. Hu, R. N. Sampaio, S. L. Marquard, M. K. Brennaman, Y. Tamaki, T. J. Meyer and G. J. Meyer, *Inorg. Chem.*, 2018, **57**, 486-494.
31. G. Li, D. Zhu, X. Wang, Z. Su and M. R. Bryce, *Chem. Soc. Rev.*, 2020, **49**, 765-838.
32. S. A. Archer, A. Raza, F. Dröge, C. Robertson, A. J. Auty, D. Chekulaev, J. A. Weinstein, T. Keane, A. J. H. M. Meijer, J. W. Haycock, S. MacNeil and J. A. Thomas, *Chem. Sci.*, 2019, **10**, 3502-3513.
33. E. Baggaley, M. R. Gill, N. H. Green, D. Turton, I. V. Sazanovich, S. W. Botchway, C. Smythe, J. W. Haycock, J. A. Weinstein and J. A. Thomas, *Angew. Chem. Int. Ed.*, 2014, **53**, 3367-3371.
34. G. Piraux, L. Bar, M. Abraham, T. Lavergne, H. Jamet, J. Dejeu, L. Marcélis, E. Defrancq and B. Elias, *Chem. Eur. J.*, 2017, **23**, 11872-11880.
35. B. A. Albani, B. Peña, S. Saha, J. K. White, A. M. Schaeffer, K. R. Dunbar and C. Turro, *Chem. Commun.*, 2015, **51**, 16522-16525.
36. S. Berardi, L. Francàs, S. Neudeck, S. Maji, J. Benet-Buchholz, F. Meyer and A. Llobet, *ChemSusChem*, 2015, **8**, 3688-3696.
37. S. Cerfontaine, S. A. M. Wehlin, B. Elias and L. Troian-Gautier, *J. Am. Chem. Soc.*, 2020, **142**, 5549-5555.
38. V. Balzani, A. Juris, M. Venturi, S. Campagna and S. Serroni, *Chem. Rev.*, 1996, **96**, 759-834.
39. A. J. Downard, G. E. Honey, L. F. Phillips and P. J. Steel, *Inorg. Chem.*, 1991, **30**, 2259-2260.
40. L. Cassidy, S. Horn, L. Cleary, Y. Halpin, W. R. Browne and J. G. Vos, *Dalton Trans.*, 2009, DOI: 10.1039/B817896H, 3923-3928.
41. Y. Halpin, L. Cleary, L. Cassidy, S. Horne, D. Dini, W. R. Browne and J. G. Vos, *Dalton Trans.*, 2009, DOI: 10.1039/B823104D, 4146-4153.
42. Y.-Q. Fang, M. I. J. Polson and G. S. Hanan, *Inorg. Chem.*, 2003, **42**, 5-7.
43. K. O. Johansson, J. A. Lotoski, C. C. Tong and G. S. Hanan, *Chem. Commun.*, 2000, DOI: 10.1039/A910257O, 819-820.
44. N. Das, G. S. Bindra, A. Paul, J. G. Vos, M. Schulz and M. T. Pryce, *Chem. Eur. J.*, 2017, **23**, 5330-5337.
45. M.-I. Takeko, T. Masahiro, M. Takayoshi and O. Tomoko, *Chem. Lett.*, 1994, **23**, 2443-2446.
46. N. H. Damrauer, T. R. Boussie, M. Devenney and J. K. McCusker, *J. Am. Chem. Soc.*, 1997, **119**, 8253-8268.
47. V. Balzani, P. Ceroni and A. Juris, in *Photochemistry and Photophysics: Concepts, Research, Applications*, Wiley-VCH, Weinheim, 2014, ch. 6.
48. N. R. Kestner, J. Logan and J. Jortner, *J. Phys. Chem.*, 1974, **78**, 2148-2166.
49. N. J. Turro, V. Ramamurthy and J. C. Scaiano, *Principles of Molecular Photochemistry—An Introduction*, University Science Books, Sausalito, CA, 2009.
50. H. Yersin, A. F. Rausch, R. Czerwieniec, T. Hofbeck and T. Fischer, *Coord. Chem. Rev.*, 2011, **255**, 2622-2652.
51. A. C. Benniston, A. Harriman, P. Li and C. A. Sams, *J. Phys. Chem. A*, 2005, **109**, 2302-2309.
52. J. V. Caspar and T. J. Meyer, *Inorg. Chem.*, 1983, **22**, 2444-2453.
53. J. V. Caspar and T. J. Meyer, *J. Am. Chem. Soc.*, 1983, **105**, 5583-5590.
54. G. H. Allen, R. P. White, D. P. Rillema and T. J. Meyer, *J. Am. Chem. Soc.*, 1984, **106**, 2613-2620.
55. J. V. Caspar, T. D. Westmoreland, G. H. Allen, P. G. Bradley, T. J. Meyer and W. H. Woodruff, *J. Am. Chem. Soc.*, 1984, **106**, 3492-3500.
56. T. C. Motley, L. Troian-Gautier, M. K. Brennaman and G. J. Meyer, *Inorg. Chem.*, 2017, **56**, 13579-13592.
57. A. Ito and T. J. Meyer, *PCCP*, 2012, **14**, 13731-13745.
58. P. G. Bradley, N. Kress, B. A. Hornberger, R. F. Dallinger and W. H. Woodruff, *J. Am. Chem. Soc.*, 1981, **103**, 7441-7446.
59. G. D. Danzer and J. R. Kincaid, *J. Phys. Chem*, 1990, **94**, 3976-3980.
60. K. Suzuki, A. Kobayashi, S. Kaneko, K. Takehira, T. Yoshihara, H. Ishida, Y. Shiina, S. Oishi and S. Tobita, *PCCP*, 2009, **11**, 9850-9860.
61. L. Hammarström, F. Barigelletti, L. Flamigni, M. T. Indelli, N. Armaroli, G. Calogero, M. Guardigli, A. Sour, J.-P. Collin and J.-P. Sauvage, *J. Phys. Chem. A*, 1997, **101**, 9061-9069.
62. A. Harriman, A. Mayeux, A. De Nicola and R. Ziessel, *PCCP*, 2002, **4**, 2229-2235.
63. R. Bensasson, C. Salet and V. Balzani, *J. Am. Chem. Soc.*, 1976, **98**, 3722-3724.
64. T. Ohno, A. Yoshimura, D. R. Prasad and M. Z. Hoffman, *J. Phys. Chem.*, 1991, **95**, 4723-4728.
65. J. K. McCusker, *Acc. Chem. Res.*, 2003, **36**, 876-887.
66. U. Lachish, P. P. Infelta and M. Grätzel, *Chem. Phys. Lett.*, 1979, **62**, 317-319.
67. C. Creutz, M. Chou, T. L. Netzel, M. Okumura and N. Sutin, *J. Am. Chem. Soc.*, 1980, **102**, 1309-1319.
68. E. König and S. Kremer, *Chem. Phys. Lett.*, 1970, **5**, 87-90.
69. G. A. Heath, L. J. Yellowlees and P. S. Braterman, *J. Chem. Soc., Chem. Commun.*, 1981, DOI: 10.1039/C39810000287, 287-289.
70. K. H. J. Buschow, J. Dieleman and G. J. Hoijtink, *The Journal of Chemical Physics*, 1965, **42**, 1993-1999.
71. R. W. Harrigan and G. A. Crosby, *The Journal of Chemical Physics*, 1973, **59**, 3468-3476.
72. M. Abrahamsson, H.-C. Becker, L. Hammarström, C. Bonnefous, C. Chamchoumis and R. P. Thummel, *Inorg. Chem.*, 2007, **46**, 10354-10364.
73. R. S. Lumpkin, E. M. Kober, L. A. Worl, Z. Murtaza and T. J. Meyer, *J. Phys. Chem.*, 1990, **94**, 239-243.
74. A. Harriman and G. Izzet, *PCCP*, 2007, **9**, 944-948.
75. J. Van Houten and R. J. Watts, *J. Am. Chem. Soc.*, 1976, **98**, 4853-4858.

76. G. D. Hager and G. A. Crosby, *J. Am. Chem. Soc.*, 1975, **97**, 7031-7037.
77. S. R. Allsopp, A. Cox, T. J. Kemp and W. J. Reed, *Journal of the Chemical Society, Faraday Transactions 1: Physical Chemistry in Condensed Phases*, 1978, **74**, 1275-1289.
78. L. S. Forster, *Coord. Chem. Rev.*, 2002, **227**, 59-92.
79. F. Barigelletti, A. Juris, V. Balzani, P. Belser and A. Von Zelewsky, *J. Phys. Chem.*, 1987, **91**, 1095-1098.
80. M. Abrahamsson, H. C. Becker and L. Hammarstrom, *Dalton Trans*, 2017, **46**, 13314-13321.
81. B. Durham, J. V. Caspar, J. K. Nagle and T. J. Meyer, *J. Am. Chem. Soc.*, 1982, **104**, 4803-4810.
82. J. K. White, R. H. Schmehl and C. Turro, *Inorg. Chim. Acta.*, 2017, **454**, 7-20.
83. E. T. Luis, H. Iranmanesh and J. E. Beves, *Polyhedron*, 2019, **160**, 1-9.
84. L. De Cola, F. Barigelletti and M. J. Cook, *Helv. Chim. Acta*, 1988, **71**, 733-741.
85. F. Barigelletti, A. Juris, V. Balzani, P. Belser and A. Von Zelewsky, *Inorg. Chem.*, 1983, **22**, 3335-3339.
86. F. Barigelletti, P. Belser, A. Von Zelewsky, A. Juris and V. Balzani, *J. Phys. Chem.*, 1985, **89**, 3680-3684.
87. F. Barigelletti, A. Juris, V. Balzani, P. Belser and A. Von Zelewsky, *J. Phys. Chem.*, 1986, **90**, 5190-5193.
88. A. Harriman, G. Izzet, S. Goeb, A. D. Nicola and R. Ziessel, *Inorg. Chem.*, 2006, **45**, 9729-9741.
89. T. E. Keyes, C. M. O'Connor, U. O'Dwyer, C. G. Coates, P. Callaghan, J. J. McGarvey and J. G. Vos, *J. Phys. Chem. A*, 1999, **103**, 8915-8920.
90. E. C. Glazer, D. Magde and Y. Tor, *J. Am. Chem. Soc.*, 2005, **127**, 4190-4192.
91. G. D. Hager, R. J. Watts and G. A. Crosby, *J. Am. Chem. Soc.*, 1975, **97**, 7037-7042.

## Graphical Abstract

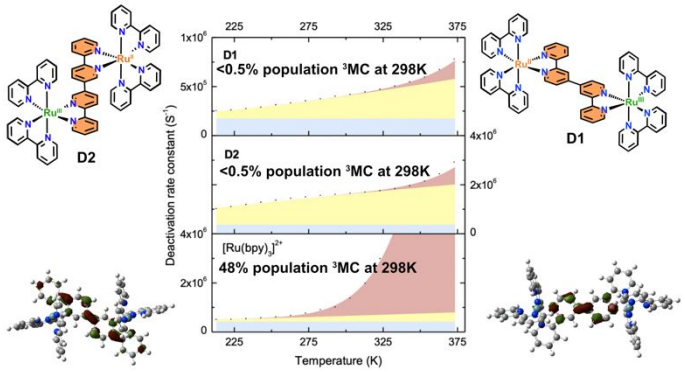


A detailed photophysical study of binuclear complexes was performed using steady-state and time-resolved photoluminescence measurements at variable temperature as well as nanosecond transient absorption spectroscopy. The results were compared with the prototypical $[Ru(bpy)_3]^{2+}$.